# Full-vectorial modal analysis for circular optical waveguides based on the multidomain Chebyshev pseudospectral method

**Rencheng Song, Jianxin Zhu,* and Xuecang Zhang**

*Department of Mathematics, Zhejiang University, Hangzhou, Zhejiang, China*
**Corresponding author: zjx@zju.edu.cn*

Received December 11, 2009; revised June 26, 2010; accepted July 5, 2010;
posted July 6, 2010 (Doc. ID 121184); published August 9, 2010

What we believe to be a new one-dimensional full-vectorial mode solver for circular waveguides in step-index optical fibers is introduced based on the multidomain Chebyshev pseudospectral method and the perfectly matched layer. The formulations are derived with two transverse components on the radial axis in the cylindrical coordinate system. The electromagnetic fields are expanded inside each homogeneous layer by the Chebyshev basis functions, and then matched rigorously at the radial discontinuities by the interface conditions. The numerical analysis on the guided and leaky modes of the two layer air-clad fiber, hybrid surface plasmon polariton, and Bragg fibers demonstrates the validity and good performance of the present method, which has remarkably high accuracy and fast convergence. © 2010 Optical Society of America

*OCIS codes:* 060.0060, 000.4430.

## 1. INTRODUCTION

The accurate calculation of full-vectorial modes of circular optical waveguides is important for the design and application of such waveguide structures in certain optical devices. In the past few decades, many numerical methods [1–7] have been proposed and widely used to solve this problem. The finite difference (FD) method is one of the most popular methods for its simplicity and flexibility. As known, one major difficulty in the FD methods is how to handle the interface conditions at the index discontinuities without losing the whole solution accuracy [4,8]. It has been verified in [8] that the commonly used average-index approximation in the conventional FD schemes has only zero-order truncation error at the interface points in the Cartesian coordinate. Recently, Lu *et al.* introduced a second order one-dimensional (1-D) full-vectorial FD mode solver [4] for circular optical waveguides. Their FD formulations are described with two transverse components $H_r$-$H_\phi$ on the radial axis in the cylindrical coordinate system, where the angular variable is separated due to the circular symmetry. In this method, the fields are rigorously matched at the radial discontinuities by the use of Taylor expansion, and the resultant matrix still keeps its compact form. Inside each homogeneous layer, the vectorial wave equations are discretized by the central FD scheme. Consequently, this FD method has second order accuracy overall. However, such a precision is still not high enough, especially in some large structures, where a great number of nodes will be needed due to the low accuracy of FD methods. Therefore, higher order methods are still important to further improve the efficiency and accuracy.

In recent years, the pseudospectral method [9–13], also called the spectral collocation method (SCM), has attracted more and more attention in computational electromagnetics (CEM) due to its high accuracy and fast convergence over the conventional methods. There is an excellent book [14] introducing this method. As known, the high order accuracy of spectral methods relies on the smoothness of solution functions [14]. Thus, a proper treatment of the interface conditions is also crucial for the spectral methods applied in CEM. In [15], Huang *et al.* first employed the multidomain pseudospectral method to analyze the modes of dielectric waveguides with step-index profiles. Their two-dimensional (2-D) formulations are introduced with two transverse components $H_x$-$H_y$ in the rectangular coordinate system. In their method, the domain is divided into several subdomains with homogeneous refractive indices. The fields in each subdomain are approximated independently by the SCM and finally connected rigorously by matching the interface conditions between the adjacent subdomains. This method has been verified to own spectral accuracy. However, it can only be used in problems with horizontal and vertical interfaces. Chiang *et al.* then proposed another mulitidomain pseudospectral frequency-domain (PSFD) scheme in [6] to determine the guided modes of general 2-D optical waveguides with arbitrary interfaces. The formulations of the PSFD method are described by $H_\xi$-$H_\eta$ in the curvilinear coordinate system. Furthermore, they also analyzed the leaky modes in [7] by incorporating the perfectly matched layer (PML) [16] with the PSFD. However, the PSFD method is not so efficient for circular optical waveguides because it does not take use of the circular symmetry.

In this study, we show the details for the first time to apply the multidomain Chebyshev pseudospectral (MCPS) method to solve the same 1-D full vectorial modal equations as in [4] under the cylindrical coordinate system. In our method, the electromagnetic fields are ex-

panded inside each homogeneous layer on the radial axis by the Chebyshev basis functions, and then matched rigorously at the radial discontinuities by the interface conditions. The PML [4,17,18] in the cylindrical coordinate system is also applied to accurately determine the guided and leaky modes. Furthermore, the generalized matrix eigenvalue problem obtained by MCPS is finally transformed into a standard one, which can be solved easily by common matrix eigenvalue solvers. The numerical analysis of the two layer air-clad fiber [6,19], hybrid surface plasmon polaritons (SPPs) [20,21], and Bragg fibers [4,22–24] shows the validity and excellent performance of our method.

This paper is organized as follows. In Section 2, we formulate the modal equations of circular optical fibers. The MCPS scheme is introduced in Section 3. Then it is validated in Section 4 by various numerical examples. Finally, we conclude this paper in Section 5.

## 2. PROBLEM FORMULATION

A quarter of the cross section of one step-index circular optical fiber is shown in Fig. 1, where the fiber is composed of piecewise homogeneous layers with refractive index $n_i$ $(i=1,2,\ldots,N)$. The radial discontinuities are denoted as $r_i$ for $i=1,2,\ldots,N-1$. Notice that the outmost infinite cladding layer with $n_N$ is enclosed at $r_N$ by the PML and $r_{\text{pml}}$ is the radius of the physical region. Thus, the thickness of the PML is $d=r_N-r_{\text{pml}}$.

The 1-D modal equations, interface, and boundary conditions for the circular waveguide were proposed in [3,4]. We also briefly introduce them here. They are expressed by the magnetic field vector $\mathbf{H}=[H_r\ H_\phi\ H_z]^T$, and the electric formulations with $\mathbf{E}=[E_r\ E_\phi\ E_z]^T$ can be obtained by a small modification on the interface conditions.

Suppose that $\mathbf{H}$ is time-harmonic and propagates along the longitudinal $z$-direction. Then it satisfies

$$\mathbf{H}(r,\phi,z)=\begin{bmatrix} H_r(r)\cos(m\phi) \\ H_\phi(r)\sin(m\phi) \\ H_z(r,\phi)\end{bmatrix}\exp[j(\omega t-\beta z)], \tag{1}$$

where $m=0,1,2,\ldots$ is the angular separation constant, $t$ is the time variable, $\omega$ is the wave frequency, and $\beta$ is the unknown propagation constant.

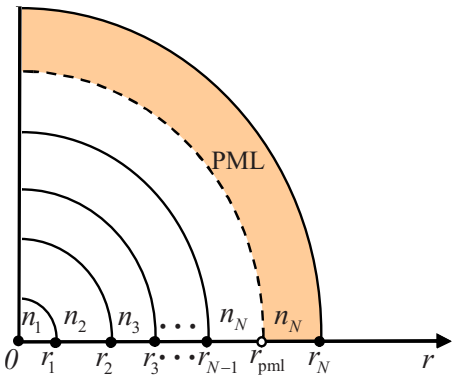


Fig. 1. (Color online) A quarter of the cross section of a step-index circular fiber.

As seen in [3,4], in the frequency domain, after reducing $H_z$ from

$$\nabla\times(\nabla\times\mathbf{H})=\kappa_0^2\varepsilon_r\mathbf{H},$$

and separating variables $\phi$ and $z$, we get the full-vectorial modal equations for circular waveguides only with the radial variable $r$,

$$\left(\frac{\mathrm{d}^2}{\mathrm{d}r^2}+\frac{1}{r}\frac{\mathrm{d}}{\mathrm{d}r}+\kappa_0^2\varepsilon_r+\frac{M}{r^2}\right)\begin{bmatrix}H_r\\H_\phi\end{bmatrix}=\beta^2\begin{bmatrix}H_r\\H_\phi\end{bmatrix}, \tag{2}$$

where $\kappa_0$ is the wavenumber of free space, $\varepsilon_r$ is the relative permittivity, and

$$M=-\begin{bmatrix}m^2+1 & 2m\\ 2m & m^2+1\end{bmatrix}.$$

For simplicity, we denote the transverse magnetic field $\left[\begin{smallmatrix}H_r\\H_\phi\end{smallmatrix}\right]$ as $\mathbf{H}$ and the transverse electric field $\left[\begin{smallmatrix}E_r\\E_\phi\end{smallmatrix}\right]$ as $\mathbf{E}$ hereafter.

As known, $\mathbf{H}$ needs to satisfy the interface conditions [4] at the radial discontinuity $r_i$, with $i=1,2,\ldots,N-1$. Namely,

$$\mathbf{H}(r_i^-)=\mathbf{H}(r_i^+), \tag{3}$$

$$\frac{\mathrm{d}\mathbf{H}(r_i^-)}{\mathrm{d}r}=\frac{(\varepsilon_{r_i^-}/\varepsilon_{r_i^+}-1)}{r_i}\begin{bmatrix}0&0\\m&1\end{bmatrix}\mathbf{H}(r_i^+)+\begin{bmatrix}1&0\\0&\varepsilon_{r_i^-}/\varepsilon_{r_i^+}\end{bmatrix}\frac{\mathrm{d}\mathbf{H}(r_i^+)}{\mathrm{d}r}, \tag{4}$$

where $\varepsilon_{r_i^-}$ and $\varepsilon_{r_i^+}$ denote the permittivities of the inner and outer media at $r_i$, respectively. These two equations are derived from the continuities of the tangential fields $H_z$ and $E_z$.

Obviously, a singularity exists at $r=0$ in Eq. (2). This is caused by the inherent property of the cylindrical coordinate system. The fields are actually bounded and smooth at this pole. So an additional boundary condition is set at $r=0$. Namely,

$$\mathbf{H}=0,\quad m\neq 1, \tag{5}$$

$$\frac{\mathrm{d}\mathbf{H}}{\mathrm{d}r}=0,\quad m=1, \tag{6}$$

at $r=0$ (see [4]).

At last, we add the PML to this model. This is done by taking a complex coordinate transform [4,17,18] on the radial variable $r$ in Eq. (2). There are

$$\frac{1}{s^2(r)}\frac{\mathrm{d}^2H_r}{\mathrm{d}r^2}+\left(\frac{1}{s(r)}\frac{\mathrm{d}}{\mathrm{d}r}\left(\frac{1}{s(r)}\right)+\frac{1}{\hat{r}s(r)}\right)\frac{\mathrm{d}H_r}{\mathrm{d}r}+\left(\kappa^2\varepsilon_r-\frac{m^2+1}{\hat{r}^2}\right)H_r-\frac{2m}{\hat{r}^2}H_\phi=\beta^2H_r, \tag{7}$$

$$\frac{1}{s^2(r)}\frac{\mathrm{d}^2H_\phi}{\mathrm{d}r^2}+\left(\frac{1}{s(r)}\frac{\mathrm{d}}{\mathrm{d}r}\left(\frac{1}{s(r)}\right)+\frac{1}{\hat{r}s(r)}\right)\frac{\mathrm{d}H_\phi}{\mathrm{d}r}+\left(\kappa^2\varepsilon_r-\frac{m^2+1}{\hat{r}^2}\right)H_\phi-\frac{2m}{\hat{r}^2}H_r=\beta^2H_\phi, \tag{8}$$

where

$$\hat{r}=\int_0^r s(t)\mathrm{d}t,\quad s(r)=\frac{\partial\hat{r}}{\partial r}=\begin{cases}1, & r<r_{\mathrm{pml}}\\ 1-j\dfrac{\sigma_r}{\omega\varepsilon_0\varepsilon_r}, & r>r_{\mathrm{pml}},\end{cases} \tag{9}$$

with $\sigma_r=\sigma_{r,\max}|r-r_{\mathrm{pml}}|^P/d^P$ and $P$ is a positive number. The maximum conductivity $\sigma_{r,\max}$ can be determined by the reflection coefficient $R$ [25], i.e.,

$$\sigma_{r,\max}=\frac{(P+1)\varepsilon_r}{2\eta_0 d}\ln\frac{1}{R}, \tag{10}$$

where $\eta_0$ is the wave impedance in free space.

As shown in [4,18,26], the PML in Eq. (9) cannot absorb the evanescent waves. One way to overcome this difficulty is to make $\sigma_r$ complex. But it will make the propagating waves oscillate faster, which exacerbates the numerical reflection [27]. Another way is to set the computational domain large enough and the evanescent waves will decay naturally. For simplicity, this paper chooses the second approach.

The zero Dirichlet boundary condition,

$$\mathbf{H}(r_N)=0, \tag{11}$$

is set on the outer boundary of the PML. Thus, the total modal equations denoted by $\mathbf{H}$ for the circular fiber are composed of Eqs. (3)–(8) and (11). And the solution domain is the closed segment $[r_0,r_N]$, where $r_0=0$.

The $\mathbf{E}$ modal equations have the same form as $\mathbf{H}$ except the interface conditions (3) and (4) are replaced with

$$\mathbf{E}(r_i^-)=\begin{bmatrix}\varepsilon_{r_i^+}/\varepsilon_{r_i^-} & 0\\ 0 & 1\end{bmatrix}\mathbf{E}(r_i^+), \tag{12}$$

$$\frac{\mathrm{d}\mathbf{E}(r_i^-)}{\mathrm{d}r}=\frac{(1-\varepsilon_{r_i^+}/\varepsilon_{r_i^-})}{r_i}\begin{bmatrix}1 & 0\\ m & 0\end{bmatrix}\mathbf{E}(r_i^+)+\frac{\mathrm{d}\mathbf{E}(r_i^+)}{\mathrm{d}r}; \tag{13}$$

see [4].

## 3. THE MCPS METHOD FOR CIRCULAR FIBER

### A. Chebyshev Differentiation Matrix

We first introduce the definition of the Chebyshev differentiation matrix [14], which is important in the Chebyshev pseudospectral method. In $[-1,1]$, the smooth function $f(x)$ can be approximated by

$$f(x)\approx\sum_{i=0}^{q}f(x_i)g_i(x), \tag{14}$$

where $g_i(x)$ is the Chebyshev–Lagrange interpolating polynomial of degree $q$, satisfying

$$g_i(x)=\frac{(1-x^2)T_q'(x)(-1)^{i+1}}{c_iq^2(x-x_i)}, \tag{15}$$

with $c_0=c_q=2$ and $c_i=1$ for $1\le i\le q-1$. The polynomial $T_q(x)$ in Eq. (15) is defined by $T_q(x)=\cos(q\cos^{-1}(x))$, where $|x|\le 1$. The node $x_i=\cos(i\pi/q)$ is the so called Chebyshev–Gauss–Lobatto point, which is also the root of $(1-x^2)T_q'(x)$.

The first order Chebyshev differentiation matrix $D_1=(d_{i,j})_{(q+1)\times(q+1)}$ on a general segment $[a,b]$ satisfies

$$\begin{bmatrix}f'(t_0)\\ f'(t_1)\\ \vdots\\ f'(t_q)\end{bmatrix}\approx D_1\begin{bmatrix}f(t_0)\\ f(t_1)\\ \vdots\\ f(t_q)\end{bmatrix}, \tag{16}$$

where

$$t_k=a+\frac{b-a}{2}(1-x_k),\quad k=0,1,\ldots,q. \tag{17}$$

Thus, $t_0=a$ and $t_q=b$. The matrix $D_1$ in Eq. (16) can be calculated by

$$d_{i,j}=-\frac{2}{b-a}\begin{cases}\frac{c_i}{c_j}\frac{(-1)^{i+j}}{x_i-x_j}, & i\neq j\\ \frac{-x_i}{2(1-x_i^2)}, & 1\le i=j\le q-1\\ \frac{2q^2+1}{6}, & i=j=0\\ -\frac{2q^2+1}{6}, & i=j=q\end{cases}; \tag{18}$$

see [28]. Similarly, the second order Chebyshev differentiation matrix $D_2$ satisfies

$$\begin{bmatrix}f''(t_0)\\ f''(t_1)\\ \vdots\\ f''(t_q)\end{bmatrix}\approx D_2\begin{bmatrix}f(t_0)\\ f(t_1)\\ \vdots\\ f(t_q)\end{bmatrix},$$

and it can be easily calculated by $D_2=D_1^2$.

### B. Discretizations of the Modal Equations by the MCPS Method

In the MCPS method, the domain $[r_0,r_N]$ is divided into subdomains $\{[r_{i-1},r_i]\}_{i=1}^N$, where the index $n_i$ is constant in $[r_{i-1},r_i]$ for $i=1,2,\ldots,N$. Suppose the degree of the Chebyshev–Lagrange interpolating polynomial on the $i$th segment $[r_{i-1},r_i]$ is $q_i$, the corresponding first and second order Chebyshev differentiation matrices are $D_1^{(i)}$ and $D_2^{(i)}$, and the discrete nodes are $\{t_k^{(i)}\}_{k=0}^{q_i}$ with $t_0^{(i)}=r_{i-1}$ and $t_{q_i}^{(i)}=r_i$. Let $\mathbf{H}_i$ and $\bar{\mathbf{H}}_i$ be

$$\mathbf{H}_i = [H_r(t_0^{(i)})\ H_r(t_1^{(i)})\ \cdots\ H_r(t_{q_i}^{(i)})\ H_\phi(t_0^{(i)})\ H_\phi(t_1^{(i)})\ \cdots\ H_\phi(t_{q_i}^{(i)})]^T, \tag{19}$$

$$\bar{\mathbf{H}}_i = [H_r(t_1^{(i)})\ H_r(t_2^{(i)})\ \cdots\ H_r(t_{q_i-1}^{(i)})\ H_\phi(t_1^{(i)})\ H_\phi(t_2^{(i)})\ \cdots\ H_\phi(t_{q_i-1}^{(i)})]^T. \tag{20}$$

The discretizations are based on the Chebyshev differentiation matrix defined before. Firstly, the modal equations (7) and (8) at $\{t_k^{(i)}\}_{k=1}^{q_i-1}$ in $(r_{i-1}, r_i)$ are discretized to

$$\begin{bmatrix} A_i & B_i \\ B_i & A_i \end{bmatrix} \mathbf{H}_i = \beta^2 \bar{\mathbf{H}}_i, \tag{21}$$

where

$$A_i = \mathrm{diag}\left(\frac{1}{s^2(t_k^{(i)})}\right) D_2^{(i)}(2{:}q_i,:) + \mathrm{diag}\left(\frac{p_k}{s(t_k^{(i)})} + \frac{1}{\hat{r}_k s(t_k^{(i)})}\right) D_1^{(i)} \times (2{:}q_i,:) + \mathrm{diag}\left(\kappa_0^2 \varepsilon_r - \frac{m^2+1}{\hat{r}_k}\right),$$

$$B_i = \mathrm{diag}\left(\frac{2m}{\hat{r}_k}\right),$$

with $p_k = (\mathrm{d}/\mathrm{d}r)[1/s(r)]|_{t_k^{(i)}}$ and $\hat{r}_k = \hat{r}|_{t_k^{(i)}}$ for $k = 1, 2, \ldots, q_i - 1$. Here $\mathrm{diag}(w_k)$ indicates the diagonal matrix with $\{w_k\}$ as the principal diagonal elements, and $D_j^{(i)}(2{:}q_i,:)$ is a MATLAB notation denoting the matrix obtained from eliminating the first and last rows of $D_j^{(i)}$ $(j = 1, 2)$.

Secondly, the interface conditions in Eqs. (3) and (4) are discretized at $r_i = t_{q_i}^{(i)}$. The Dirichlet equation (3) is discretized to

$$\mathbf{H}(t_{q_i}^{(i)}) = \mathbf{H}(t_0^{(i+1)}), \tag{22}$$

and the two components of the Neumann equation (4) are discretized to

$$\sum_{j=1}^{q_i+1} D_1^{(i)}(q_i+1, j) H_r(t_{j-1}^{(i)}) = \sum_{j=1}^{q_{i+1}+1} D_1^{(i+1)}(1, j) H_r(t_{j-1}^{(i+1)}), \tag{23}$$

$$\sum_{j=1}^{q_i+1} D_1^{(i)}(q_i+1, j) H_\phi(t_{j-1}^{(i)}) = \frac{m(\varepsilon_{r_i^-}/\varepsilon_{r_i^+} - 1)}{r_i} H_r(t_0^{(i+1)}) + \frac{(\varepsilon_{r_i^-}/\varepsilon_{r_i^+} - 1)}{r_i} H_\phi(t_0^{(i+1)}) + \frac{\varepsilon_{r_i^-}}{\varepsilon_{r_i^+}} \sum_{j=1}^{q_{i+1}+1} D_1^{(i+1)}(1, j) H_\phi(t_{j-1}^{(i+1)}). \tag{24}$$

Finally, at $r = r_0 = t_0^{(1)}$, we get

$$\mathbf{H}(t_0^{(1)}) = 0, \quad m \neq 1, \tag{25}$$

$$\sum_{j=1}^{q_1+1} D_1^{(1)}(1, j) \mathbf{H}(t_{j-1}^{(1)}) = 0, \quad m = 1, \tag{26}$$

and at $r = r_N = t_{q_N}^{(N)}$ there is

$$\mathbf{H}(t_{q_N}^{(N)}) = 0. \tag{27}$$

Those discrete equations for **E** formulations are similar to those of **H** and are omitted here.

### C. The Reformulation of the Matrix Eigenvalue Problem

Let $\mathbf{H}_T = [\mathbf{H}_1^T\ \mathbf{H}_2^T\ \cdots\ \mathbf{H}_N^T]^T$, where $\mathbf{H}_i$ is the column vector in Eq. (19) for $i = 1, 2, \ldots, N$. A generalized matrix eigenvalue problem,

$$S\mathbf{H}_T = \beta^2 B \mathbf{H}_T, \tag{28}$$

is obtained by assembling the discrete equations (21)–(27) under the sequence of $\mathbf{H}_T$, where $S$ is a square block sparse coefficient matrix of unknowns and $B$ is the modified identity matrix whose partial principal diagonal elements are replaced with zeros at those boundary and interface nodes.

Huang pointed out in [29] that Eq. (28) can be solved directly by the implicitly restarted Arnoldi method, which is efficient for sparse and large matrices. However, we find that it is more stable and accurate to reduce Eq. (28) to a standard matrix eigenvalue problem.

For conciseness, we take $S$ as a $4\times4$ matrix to show the detailed procedure. Suppose

$$\begin{bmatrix} s_{11} & s_{12} & s_{13} & s_{14} \\ s_{21} & s_{22} & s_{23} & s_{24} \\ s_{31} & s_{32} & s_{33} & s_{34} \\ s_{41} & s_{42} & s_{43} & s_{44} \end{bmatrix} \begin{bmatrix} H_1 \\ H_2 \\ H_3 \\ H_4 \end{bmatrix} = \beta^2 \begin{bmatrix} 1 & & & \\ & 1 & & \\ & & 0 & \\ & & & 1 \end{bmatrix} \begin{bmatrix} H_1 \\ H_2 \\ H_3 \\ H_4 \end{bmatrix}. \tag{29}$$

If $H_4 = 0$ is known in Eq. (29), e.g., the zero Dirichlet condition, we can eliminate its corresponding row and column, namely,

$$\begin{bmatrix} s_{11} & s_{12} & s_{13} \\ s_{21} & s_{22} & s_{23} \\ s_{31} & s_{32} & s_{33} \end{bmatrix} \begin{bmatrix} H_1 \\ H_2 \\ H_3 \end{bmatrix} = \beta^2 \begin{bmatrix} 1 & & \\ & 1 & \\ & & 0 \end{bmatrix} \begin{bmatrix} H_1 \\ H_2 \\ H_3 \end{bmatrix}. \tag{30}$$

Furthermore, from the last row of Eq. (30), there is $H_3 = -(s_{31}/s_{33})H_1 - (s_{32}/s_{33})H_2$. Substituting it into the first two rows and doing some simplifications, we get

$$\tilde{S}_{2\times2} \begin{bmatrix} H_1 \\ H_2 \end{bmatrix} = \beta^2 \begin{bmatrix} H_1 \\ H_2 \end{bmatrix}. \tag{31}$$

Equation (31) is a standard matrix eigenvalue problem with the eigenvector $[H_1\ H_2]^T$.

The above elimination process is similar to those done in [14,30], and it can be done locally since $S$ is a block

sparse matrix. After finishing all the recursive eliminations of interface and boundary nodes, we get a standard matrix eigenvalue problem

$$\tilde{S}\begin{bmatrix}\bar{\mathbf{H}}_1\\ \bar{\mathbf{H}}_2\\ \vdots\\ \bar{\mathbf{H}}_N\end{bmatrix}=\beta^2\begin{bmatrix}\bar{\mathbf{H}}_1\\ \bar{\mathbf{H}}_2\\ \vdots\\ \bar{\mathbf{H}}_N\end{bmatrix}, \tag{32}$$

where $\tilde{S}$ is the reduction matrix of $S$ and $\bar{\mathbf{H}}_i$ is the column vector in Eq. (20). Equation (32) can be solved by the commonly used matrix eigenvalue solver.

## 4. NUMERICAL EXAMPLES AND DISCUSSIONS

### A. Two Layer Air-Clad Optical Fiber

In this section, several numerical examples are studied to show the validity and performance of our method, of which the solution accuracy and convergence are mainly investigated and compared with other methods.

A two layer ($N=2$) air-clad optical fiber [6] is studied first. Its analytical effective index $n_{\text{eff}}=\beta/\kappa_0$ can be obtained from the nonlinear dispersion relation by the Newton root finding technique [19]. From Fig. 1, the parameters of this fiber are $r_1=0.6$ $\mu$m with the core index $n_1=\sqrt{8}$, and the air cladding index $n_2=1.0$ with $r_2=6.5$ $\mu$m. The PML parameters are $r_{\text{pml}}=5.0$ $\mu$m, $P=4$, $R=10^{-8}$. In fact, as seen in [6], there is no need to use PML here if we are interested only in guiding modes. But the PML is necessary if we also want to compute the leaky modes. To be unified, all the examples studied in this paper are calculated under PMLs.

In this example, the number $q_i$ of the discrete nodes in the $i$th segment $[r_{i-1},r_i]$ is determined by

$$q_i=\left\lfloor T\cdot\left(\frac{\alpha_i}{\sum_{i=1}^{N}\alpha_i}\right)\right\rfloor,\quad i=1,2, \tag{33}$$

where $T$ is a given integer, $\lfloor\ \rfloor$ denotes the floor, and $\alpha_i=[(r_i-r_{i-1})/r_N]|n_i|$. Suppose that the order of $\tilde{S}$ in Eq. (32) is $U$, which indicates the number of unknowns.

First, we verify the validity of the MCPS method. The effective index $n_{\text{eff}}$ of the fundamental mode $\text{HE}_{11}$ of this fiber is shown in Fig. 2 with different wavelengths $\lambda$. It can be seen the numerical results (dotted line) obtained by the MCPS method agree well with the exact ones (solid line).

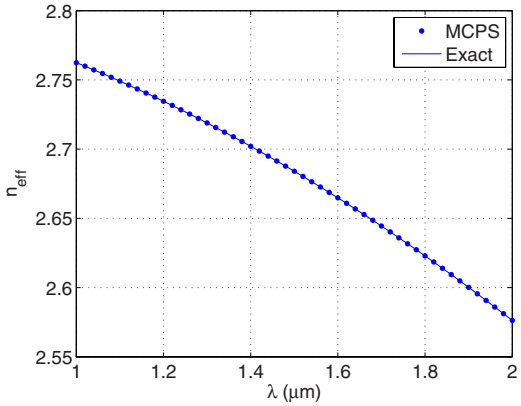


Fig. 2. (Color online) The effective index of the $\text{HE}_{11}$ mode for the two layer optical fiber with different $\lambda$'s.

Then we study its solution accuracy. Suppose the wavelength $\lambda=1.5$ $\mu$m. The exact effective index of the $\text{HE}_{11}$ mode is $n_{\text{eff,exact}}=2.684\ 019\ 321\ 601\ 08$ [6]. In Table 1, we show the numerical $n_{\text{eff}}$ obtained by both the electric and magnetic formulations. It can be seen the numerical $n_{\text{eff}}$ achieves up to 12 digits when $U=114$ and the solution results of the two formulations are almost the same. By comparison, similar precision (11 digits) of $n_{\text{eff}}$ was achieved in PSFD [6] with 4840 unknowns. Correspondingly, the computing time of MCPS at $U=114$ is only 0.1825 s on a personal computer with an Intel Pentium 4 3.0 GHz central processing unit (CPU), while that of the PSFD [6] takes more than 52 s with an Intel Dual Core 4300 1.8 GHz CPU. Obviously, the 1-D MCPS method is more efficient compared to the 2-D PSFD method in [6] for the circular waveguide.

Finally, we consider the convergence of the MCPS method. The relative error is defined by

$$\text{Relative error}=\frac{|n_{\text{eff}}-n_{\text{eff,exact}}|}{|n_{\text{eff,exact}}|}, \tag{34}$$

where $n_{\text{eff}}$ is the numerical effective index. In Fig. 3, the convergence curves of the MCPS method are shown to compare with that of the FD method in [4]. It can be seen that our MCPS method converges much faster and the performances of its $H$ and $E$ formulations are identical. Actually, the FD method in [4] has $O(h^2)$ convergence rate, where $h=(r_N-r_0)/K$ is the step size with $K$ as the number of discrete nodes. But the spectral methods usually have the typical convergence rate $O(c^K)$ $(0<c<1)$ to approximate the analytical functions [14]. Thus, to reach the same precision, the number of nodes needed in MCPS is much less than the FD in [4]. On the other hand, if the

**Table 1. The Numerical $n_{\text{eff}}$ of $\text{HE}_{11}$ Mode ($m=1$) by MCPS for Air-Clad Optical Fiber**

| $T$ | $U$ | $n_{\text{eff}}(\mathbf{E})$ | $n_{\text{eff}}(\mathbf{H})$ |
|---|---|---|---|
| 10 | 14 | $2.710\ 234\ 122\ 200\ 30-7.85\times10^{-7}i$ | $2.710\ 234\ 122\ 200\ 30-7.85\times10^{-7}i$ |
| 20 | 34 | $2.684\ 394\ 856\ 970\ 74+3.11\times10^{-8}i$ | $2.684\ 394\ 856\ 970\ 74+3.11\times10^{-8}i$ |
| 30 | 54 | $2.684\ 023\ 848\ 731\ 34+6.33\times10^{-10}i$ | $2.684\ 023\ 848\ 731\ 34+6.33\times10^{-10}i$ |
| 40 | 74 | $2.684\ 019\ 330\ 566\ 38+1.75\times10^{-12}i$ | $2.684\ 019\ 330\ 566\ 40+1.75\times10^{-12}i$ |
| 50 | 94 | 2.684 019 321 620 47 | 2.684 019 321 620 47 |
| 60 | 114 | 2.684 019 321 608 19 | 2.684 019 321 608 18 |

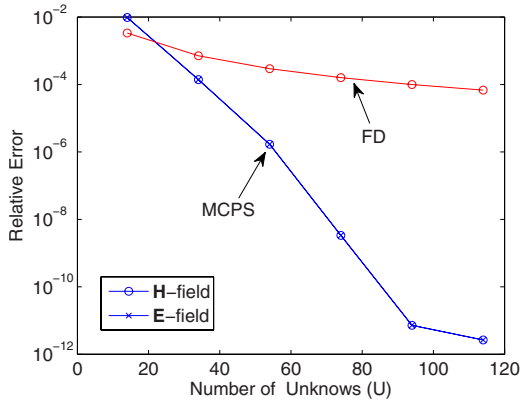


Fig. 3. (Color online) The convergence curves of the $HE_{11}$ mode by MCPS compared with the FD in [4] for the air-clad optical fiber.

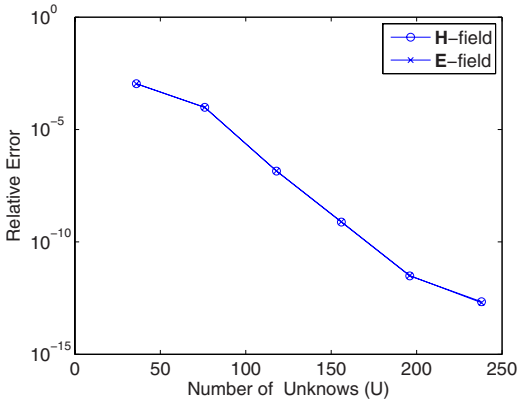


Fig. 4. (Color online) The convergence curves of the antisymmetric mode ($m=4$) by MCPS for hybrid SPP.

same number of nodes are used, a much higher order of accuracy can be obtained by MCPS.

### B. The Optical Fiber Hybrid Surface Plasmon Polariton

We study the optical fiber hybrid SPP [4,20] here to verify the effectiveness of the MCPS method for circular waveguides in lossy materials. A typical hybrid SPP is composed of three different layers ($N=3$) of materials. As seen in Fig. 1, the core index $n_1=1.515$ and the core radius $r_1$ satisfy $\kappa_0 r_1=5.0$. The second layer is silver with the relative permittivity $\varepsilon_r=-19+0.53i$ ($n_2=\varepsilon_r^{1/2}$) at the wavelength of $\lambda=0.6328$ $\mu$m, and $r_2$ satisfies $\kappa_0(r_2-r_1)=0.6$. The index of the cladding layer is $n_3=1.500$ and $r_3=r_{\text{pml}}+d$ $\mu$m. The PML parameters are same as the two layer fiber studied before except $r_{\text{pml}}=6.0$ $\mu$m.

Since the thin metal layer of the hybrid SPP has significant influence on the effective index, the node distribution in this layer must be denser than the other two layers. In this example, the node number $q_i$ of the $i$th segment $[r_{i-1},r_i]$ is determined by

$$q_i=\lceil T\alpha_i\rceil, \quad i=1,2,3, \tag{35}$$

where $T$ is a given integer, $\lceil\ \rceil$ denotes the ceil, and $\alpha=[0.147\ \ 0.118\ \ 0.735]$.

When $m=4$, the analytical $n_{\text{eff}}$ of the antisymmetric mode is $1.506\,444+3.663\times10^{-3}i$ [20]. It was also solved as $1.506\,444+3.662\,701\times10^{-3}i$ by the FD method in [4]. In Table 2, we compute it by MCPS with different $T$'s under the PML parameters $d=1.0$ $\mu$m and $R=10^{-8}$. It can be seen $n_{\text{eff}}$ of MCPS at $T=60$ has similar accuracy as that of the FD method. Since the MCPS solutions converge, $n_{\text{eff}}$ at $T=120$ is certainly more accurate than $T=60$. To make sure of its reachable digits, a high-precision reference solution is needed. We compute it through the MCPS method with enough nodes. In fact, $T=200$ and $T=300$ under the following PML parameters:

- $R=10^{-8}$ and $d=0.2j$ $\mu$m, $j=1,2,\ldots,10$;
- $R=10^{-12}$ and $d=0.2j$ $\mu$m, $j=1,2,\ldots,10$;
- $d=1.0$ $\mu$m and $R=10^{-2j}$, $j=2,3,\ldots,7$,

are considered. In this way, we obtain the credible $n_{\text{eff}}$ of the antisymmetric mode ($m=4$) as $1.506\,443\,741\,3+3.662\,698\,058\times10^{-3}i$. Thus, the results of the antisymmetric mode ($m=4$) in Table 2 are believed to have eleven exact digits in real part and ten accurate digits in imaginary part.

Finally, we consider the convergence rate of the MCPS method for this example. Let the MCPS result with $T=200$ ($U=396$) be the reference solution. The PML parameters are fixed as $d=1$ $\mu$m and $R=10^{-8}$. This is because other PML parameters lead to similar convergence results. In Fig. 4, we observe the spectral convergence behavior, where the smallest relative error achieves $O(10^{-12})$ at $U=238$. The convergence rates of the two formulations are almost identical.

### C. The Bragg Fibers

The Bragg fibers [4,22–24] attract more and more attention due to their special properties of guiding light. They are studied here to show the performance of the MCPS method in the super-multi-interface structures. As known, a typical hollow core Bragg fiber is composed of an air-core, several periodic pairs of alternating materials, and an outmost infinite cladding layer.

The parameters of two Bragg fibers [4,24] are introduced in Table 3, where $n_1$ is the air-core index; $n_2$ and $n_3$ are, respectively, the high and low indices of the first pe-

**Table 2. The Numerical $n_{\text{eff}}$ of Antisymmetric Mode ($m=4$) by MCPS for Hybrid SPP**

| $T$ | $U$ | $n_{\text{eff}}(\mathbf{E})$ | $n_{\text{eff}}(\mathbf{H})$ |
|---|---|---|---|
| 20 | 36 | $1.504\,873\,354\,739\,528+4.079\,641\,634\,744\times10^{-3}i$ | $1.504\,843\,652\,588\,878+4.076\,213\,008\,938\times10^{-3}i$ |
| 40 | 76 | $1.506\,299\,567\,238\,919+3.665\,911\,796\,684\times10^{-3}i$ | $1.506\,297\,785\,778\,939+3.665\,763\,504\,535\times10^{-3}i$ |
| 60 | 118 | $1.506\,443\,523\,479\,754+3.662\,701\,351\,070\times10^{-3}i$ | $1.506\,443\,527\,907\,785+3.662\,701\,557\,772\times10^{-3}i$ |
| 80 | 156 | $1.506\,443\,740\,128\,931+3.662\,698\,102\,403\times10^{-3}i$ | $1.506\,443\,740\,170\,344+3.662\,698\,103\,466\times10^{-3}i$ |
| 100 | 196 | $1.506\,443\,741\,314\,853+3.662\,698\,058\,128\times10^{-3}i$ | $1.506\,443\,741\,314\,997+3.662\,698\,058\,130\times10^{-3}i$ |
| 120 | 238 | $1.506\,443\,741\,319\,942+3.662\,698\,058\,103\times10^{-3}i$ | $1.506\,443\,741\,319\,974+3.662\,698\,058\,102\times10^{-3}i$ |

**Table 3. Parameters of two Bragg Fibers**

| ID | $n_1$ | $n_2$ | $n_3$ | $n_N$ | $r_1$ ($\mu$m) | $\delta_1$ ($\mu$m) | $\delta_2$ ($\mu$m) | $N_{\text{pair}}$ | $N$ |
|---|---|---|---|---|---|---|---|---|---|
| (a) | 1.0 | 1.49 | 1.17 | 1.49 | 1.3278 | 0.2133 | 0.3460 | 16 | 34 |
| (b) | 1.0 | 1.45 | 1.10 | 1.45 | 2.0 | 0.5 | 0.5 | 50 | 102 |

**Table 4. The Numerical $n_{\text{eff}}$ of $\text{TE}_{01}$ Mode ($m=0$) by MCPS for Bragg Fiber (a)**

| $T$ | $U$ | $n_{\text{eff}}(\mathbf{E})$ | $n_{\text{eff}}(\mathbf{H})$ |
|---|---|---|---|
| 200 | 346 | $0.891\,692\,470\,534\,612-1.224\,474\,1\times10^{-8}i$ | $0.891\,692\,470\,534\,627-1.224\,473\,9\times10^{-8}i$ |
| 300 | 568 | $0.891\,062\,513\,765\,067-1.426\,342\,3\times10^{-8}i$ | $0.891\,062\,513\,765\,046-1.426\,342\,7\times10^{-8}i$ |
| 400 | 758 | $0.891\,066\,997\,011\,825-1.422\,152\,0\times10^{-8}i$ | $0.891\,066\,997\,011\,910-1.422\,152\,1\times10^{-8}i$ |
| 500 | 980 | $0.891\,067\,218\,043\,187-1.422\,606\,8\times10^{-8}i$ | $0.891\,067\,218\,043\,118-1.422\,607\,2\times10^{-8}i$ |
| 600 | 1170 | $0.891\,067\,217\,430\,514-1.422\,605\,2\times10^{-8}i$ | $0.891\,067\,217\,430\,386-1.422\,605\,5\times10^{-8}i$ |
| 700 | 1360 | $0.891\,067\,217\,466\,421-1.422\,604\,9\times10^{-8}i$ | $0.891\,067\,217\,466\,790-1.422\,604\,7\times10^{-8}i$ |

**Table 5. The $n_{\text{eff}}$ of Higher Order Modes of Bragg Fiber (a) Calculated by Different Methods**

| | $\text{TM}_{01}$ ($m=0$) | Hybrid ($m=1$) |
|---|---|---|
| MCPS ($T=700$) | $0.792\,085\,903\,112\,979-1.819\,323\,186\,129\times10^{-3}i$ | $0.805\,577\,881\,426\,740-1.739\,146\,908\,714\times10^{-3}i$ |
| Improved FD [4] | $0.792\,095-1.8191\times10^{-3}i$ | $0.805\,582-1.7389\times10^{-3}i$ |
| FD frequency domain [2] | N/A | $0.805\,583-1.7375\times10^{-3}i$ |
| Chew's method [31] | $0.792\,086-1.8190\times10^{-3}i$ | $0.805\,578-1.7392\times10^{-3}i$ |

riodic pair of materials in the second and third layers; $n_N$ is the index of the outmost infinite cladding layer; $r_1$ is the core radius; $\delta_1$ ($=r_2-r_1$) and $\delta_2$ ($=r_3-r_2$) are, respectively, the thicknesses of the second and third layers; $N_{\text{pair}}$ is the number of periodic pairs; and $N$ ($=2N_{\text{pair}}+2$) is total number of layers (see Fig. 1). The outmost infinite cladding layers of the two fibers are truncated by PMLs with $r_{\text{pml}}=r_1+N_{\text{pair}}(\delta_1+\delta_2)+5$ $\mu$m and $r_N=r_{\text{pml}}+d$ $\mu$m.

In the two examples, the node number $q_i$ of the $i$th segment $[r_{i-1},r_i]$ is determined by the following rule:

$$q_i=\left\lceil T\left(\frac{\alpha_i}{\sum_{i=1}^{N}\alpha_i}\right)\right\rceil,\quad i=1,2,\ldots,N, \tag{36}$$

where $T$ is a given integer, $\lceil\ \rceil$ denotes the ceil, and $\alpha_i=[(r_i-r_{i-1})/r_N]|n_i|$.

Different from the two layer fiber studied before, the fundamental mode of the Bragg fiber is the $\text{TE}_{01}$ mode and it has the lowest loss compared to other higher order modes. Suppose the wavelength $\lambda=1.0$ $\mu$m. For Bragg fiber (a), $n_{\text{eff}}$ of its fundamental mode was solved as $0.891\,068-1.4227\times10^{-8}i$ in [4] by the FD method. Another earlier result was $0.891\,067-1.4226\times10^{-8}i$ by Chew's method [31]. In Table 4, we show our MCPS results under the PML parameters $d=1.0$ $\mu$m and $R=10^{-8}$. It can be seen that the MCPS solutions are closer to those of Chew's method [31]. In order to make sure of the reachable digits, we use the same method as the hybrid SPP but with $T=1200$ to compute the reference solutions for the modes of Bragg fiber (a). In this way, we obtain the credible $n_{\text{eff}}$ of the $\text{TE}_{01}$ mode as $0.891\,067\,217\,4-1.422\,60\times10^{-8}i$. Thus, the MCPS results in Table 4 with $T=700$ are believed to have ten accurate digits in real part and six exact digits in imaginary part. To achieve

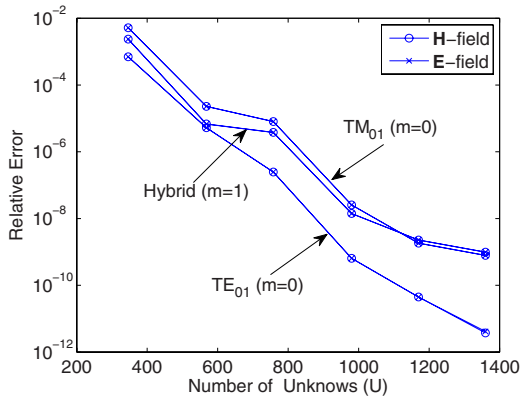


Fig. 5. (Color online) The convergence curves of the modes by MCPS for Bragg fiber (a).

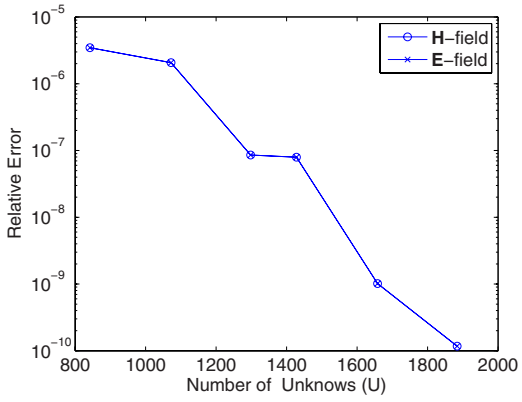


Fig. 6. (Color online) The convergence curves of the $\text{TE}_{01}$ mode ($m=0$) by MCPS for Bragg fiber (b).

**Table 6. The Propagation Constant $\beta$ of the $TE_{01}$ Mode ($m=0$) by MCPS for Bragg Fiber (b)**

| $T$ | $U$ | $\beta(\mathbf{E})$ | $\beta(\mathbf{H})$ |
|---|---|---|---|
| 500 | 842 | $2.512\,645\,016\,906\,381+1.1\times10^{-14}i$ | $2.512\,645\,016\,906\,348+4.0\times10^{-15}i$ |
| 600 | 1072 | $2.512\,648\,540\,225\,474-1.9\times10^{-14}i$ | $2.512\,648\,540\,225\,040-1.9\times10^{-14}i$ |
| 700 | 1298 | $2.512\,653\,950\,400\,662-2.2\times10^{-14}i$ | $2.512\,653\,950\,400\,798+7.0\times10^{-15}i$ |
| 800 | 1428 | $2.512\,653\,535\,595\,115+1.7\times10^{-14}i$ | $2.512\,653\,535\,595\,069-8.0\times10^{-15}i$ |
| 900 | 1658 | $2.512\,653\,737\,717\,467-3.5\times10^{-14}i$ | $2.512\,653\,737\,717\,334-1.1\times10^{-14}i$ |
| 1000 | 1884 | $2.512\,653\,735\,463\,200-1.0\times10^{-15}i$ | $2.512\,653\,735\,463\,253+4.4\times10^{-14}i$ |

similar precision as the FD result, only eight nodes in the thinner $\delta_1$ layer are needed in MCPS ($T=500$), while it is 100 for that of the FD in [4]. So it indicates again that the MCPS converges much faster than the FD method.

Other higher order modes such as the $TM_{01}$ ($m=0$) and the hybrid ($m=1$) modes are also calculated by MCPS for Bragg fiber (a). To be concise, only $n_{\text{eff}}$ at $T=700$ with the PML parameters $d=1.0$ $\mu$m and $R=10^{-8}$ is shown and compared with the known results in Table 5. Good agreement is observed on these data. The reference solutions of these two modes are also computed in the same way as the $TE_{01}$ mode. The credible effective index of $TM_{01}$ mode is $0.792\,085\,903-1.819\,322\times10^{-3}i$. It can be seen that the MCPS result with $T=700$ has nine exact digits in real part and six exact digits in imaginary part. Similarly, the credible $n_{\text{eff}}$ of the hybrid mode ($m=1$) is $0.805\,577\,881-1.739\,146\times10^{-3}i$. Thus, the result of the hybrid mode in Table 5 has nine exact digits in real part and seven accurate digits in imaginary part.

Then we study the convergence rates of MCPS to solve these three modes. The reference solutions are all obtained by MCPS at $T=1200$ ($U=2374$). The PML parameters are fixed as $d=1$ $\mu$m and $R=10^{-8}$. The convergence curves are shown in Fig. 5, where the spectral convergence is observed. Particularly, the convergence rate of the $TE_{01}$ mode is a little faster that the other two modes. It indicates that more nodes are needed in the higher order modes than the fundamental mode if the same order of precision is desired.

The Bragg fiber (b) [24] has more periodic pairs than the Bragg fiber (a). Suppose the wavelength $\lambda=2.0$ $\mu$m. The analytical propagation constant of the $TE_{01}$ mode of Bragg fiber (b) is $\beta_{\text{exact}}=2.512\,653\,735\,168\,542$ [24]. Suppose that the PML parameters are fixed as $d=1$ $\mu$m and $R=10^{-8}$. In Table 6, we show the numerical results of $\beta$ by the MCPS method. The imaginary parts of $\beta$ are on the order of $10^{-14}$, which indicates that the $TE_{01}$ mode is a quasi-guided mode with a very low loss. When $T=1000$, nine accurate digits after the decimal point are obtained, while only eight nodes are used in the $\delta_2$ layer. The convergence curve of the $TE_{01}$ mode for Bragg fiber (b) is shown in Fig. 6, where the quasi-spectral convergence is observed.

## 5. CONCLUSION

We have proposed a new 1-D full-vectorial mode solver based on the multidomain Chebyshev pseudospectral (MCPS) method for the circular waveguides. Numerical studies have verified its validity and performance. We see that the MCPS solutions have quasi-spectral convergence rate and they agree well with the known results. Particularly, compared to the FD method in [4], a much higher order of solution accuracy is achieved in the MCPS method with even less nodes. And the MCPS method is also more efficient than the PSFD method in [6] due to its lower dimension advantage. In addition, the indiscernible difference on the performance of the electric and magnetic MCPS formulations shows its self-consistency. Although the MCPS method is described only for step-index circular optical waveguides in this paper, we also indicate that it can be easily extended to the graded index ones if we replace the constant $\kappa_0^2\varepsilon_r$ with $\kappa_0^2\varepsilon_r(t_k^{(i)})$ in the discrete equations.

## ACKNOWLEDGMENTS

The authors thank Professor Li Yang and Dr. Yuchun Lu for their valuable suggestions and discussions.

## REFERENCES

1. C. C. Su and C. H. Chen, "Calculation of propagation constants and cutoff frequencies of radially inhomogeneous optical fibers," IEEE Trans. Microwave Theory Tech. **MTT-34**, 328–332 (1986).
2. F. Wu, S. Guo, K. Ikram, S. Albin, H. Tai, and R. S. Rogowski, "Numerical analysis of Bragg fibers using a compact 1-D finite-difference frequency-domain method," Opt. Commun. **249**, 165–174 (2005).
3. L. Yang, K. Jiang, C. L. Xu, and W. P. Huang, "A highly efficient and accurate full vector solver for guided and leaky modes of optical fibers," Proc. SPIE **6343**, 63431C (2006).
4. Y. C. Lu, L. Yang, W. P. Huang, and S. S. Jian, "Improved full-vector finite-difference complex mode solver for optical waveguides of circular symmetry," J. Lightwave Technol. **26**, 1868–1876 (2008).
5. U. Langbein, U. Trutschel, A. Unger, and M. Y. C. Duguay, "Rigorous mode solver for multilayer cylindrical waveguide structures using constraints optimization," Opt. Quantum Electron. **41**, 223–233 (2009).
6. P. J. Chiang, C. L. Wu, C. H. Teng, C. S. Yang, and H. C. Chang, "Full-vectorial optical waveguide mode solvers using multidomain pseudospectral frequency-domain (PSFD) formulations," IEEE J. Quantum Electron. **44**, 56–66 (2008).
7. P. J. Chiang and H. C. Chang, "Analysis of leaky optical waveguides using pseudospectral methods," in *Integrated Photonics Research and Applications/Nanophotonics* (Optical Society of America, 2006), paper ITuA3.
8. Y. P. Chiou, Y. C. Chiang, and H. C. Chang, "Improved three-point formulas considering the interface conditions in the finite-difference analysis of step-index optical devices," J. Lightwave Technol. **18**, 243–251 (2000).
9. B. Yang, D. Gottlieb, and J. S. Hesthaven, "Spectral simulations of electromagnetic wave scattering," J. Comput.

Phys. **134**, 216–230 (1997).
10. B. Yang and J. S. Hesthaven, "A pseudospectral method for time-domain computation of electromagnetic scattering by bodies of revolution," IEEE Trans. Antennas Propag. **47**, 132–141 (1999).
11. J. S. Hesthaven, P. G. Dinesen, and J. P. Lynov, "Spectral collocation time-domain modeling of diffractive optical elements," J. Comput. Phys. **155**, 287–306 (1999).
12. G. Zhao and Q. H. Liu, "The 3-D multidomain pseudospectral time-domain algorithm for inhomogeneous conductive media," IEEE Trans. Antennas Propag. **52**, 742–749 (2004).
13. Q. H. Liu, "A pseudospectral frequency-domain (PSFD) method for computational electromagnetics," IEEE Antennas Wireless Propag. Lett. **1**, 131–134 (2002).
14. L. N. Trefethen, *Spectral Methods in Matlab* (SIAM, 2000).
15. C. C. Huang, C. C. Huang, and J. Y. Yang, "A full-vectorial pseudospectral modal analysis of dielectric optical waveguides with stepped refractive index profiles," IEEE J. Sel. Top. Quantum Electron. **11**, 457–465 (2005).
16. J. P. Berenger, "A perfectly matched layer for the absorption of electromagnetic waves," J. Comput. Phys. **114**, 185–200 (1994).
17. W. Chew, J. Jin, and E. Michielssen, "Complex coordinate stretching as a generalized absorbing boundary condition," Microwave Opt. Technol. Lett. **15**, 363–369 (1997).
18. N. N. Feng, G. R. Zhou, C. Xu, and W. P. Huang, "Computation of full-vector modes for bending waveguide using cylindrical perfectly matched layers," J. Lightwave Technol. **20**, 1976–1980 (2002).
19. L. M. Tong, J. Y. Lou, and E. Mazur, "Single-mode guiding properties of subwavelength-diameter silica and silicon wire waveguides," Opt. Express **12**, 1025–1035 (2004).
20. S. J. Al-Bader and M. Imtaar, "Optical fiber hybrid-surface plasmon polaritons," J. Opt. Soc. Am. B **10**, 83–88 (1993).
21. Y. J. He, Y. L. Lo, and J. F. Huang, "Optical-fiber surface-plasmon-resonance sensor employing long-period fiber gratings in multiplexing," J. Opt. Soc. Am. B **23**, 801–811 (2006).
22. Y. Xu, G. X. Ouyang, R. K. Lee, and A. Yariv, "Asymptotic matrix theory of Bragg fibers," J. Lightwave Technol. **20**, 428–440 (2002).
23. W. Mohammed, X. Gu, and P. W. E. Smith, "Full vectorial modal analysis of specialty fibers and their Bragg grating characterization," Appl. Opt. **45**, 3307–3316 (2006).
24. M. N. Ji, Z. D. Shi, and Q. Guo, "Mode characteristics of hollow core Bragg fiber," Chin. Opt. Lett. **3**, 132–135 (2005).
25. C. P. Yu and H. C. Chang, "Applications of the finite difference frequency domain mode solution method to photonic crystal structures," in *Electromagnetic Theory and Applications for Photonic Crystals*, K. Yasumoto, ed. (Taylor & Francis Group, 2006), pp. 351–397.
26. J. Y. Fang and Z. H. Wu, "Generalized perfectly matched layer for the absorption of propagating and evanescent waves in lossless and lossy media," IEEE Trans. Microwave Theory Tech. **44**, 2216–2222 (1996).
27. S. G. Johnson, *Notes on Perfectly Matched Layers (PMLs)* (Massachusetts Institute of Technology, 2008).
28. L. J. Yuan and Y. Y. Lu, "An efficient bidirectional propagation method based on Dirichlet-to-Neumann maps," IEEE Photon. Technol. Lett. **18**, 1967–1969 (2006).
29. C. C. Huang, "Improved pseudospectral mode solver by prolate spheroidal wave functions for optical waveguides with step-index," J. Lightwave Technol. **27**, 597–605 (2009).
30. P. J. Chiang, C. P. Yu, and H. C. Chang, "Analysis of two-dimensional photonic crystals using a multidomain pseudospectral method," Phys. Rev. E **75**, 026703 (2007).
31. W. C. Chew, *Waves and Fields in Inhomogeneous Media* (Springer, 1990).